11th Canadian Masonry Symposium, Toronto, Ontario, May 31- June 3, 2009

EFFECTS OF BEARING GEOMETRY ON BASE ISOLATION CHARACTERISTICS FOR MASONRY STRUCTURES

H. Toopchi-Nezhad[1], M.J. Tait[2], and R.G. Drysdale[3]

[1] Post Doctoral Fellow, Department of Civil Engineering, McMaster University, Hamilton, ON, L8S 4L7, Canada, toopchh@mcmaster.ca

[2] Assistant Professor, Department of Civil Engineering, McMaster University, taitm@mcmaster.ca

[3] Professor Emeritus, Department of Civil Engineering, McMaster University, drysdale@mcmaster.ca

ABSTRACT

Stable unbonded-fiber reinforced elastomeric isolator (SU-FREI) bearings have been designed for earthquake protection of relatively rigid masonry low rise buildings. They exhibit rollover deformation under lateral loads due to both the unbonded boundary conditions of the bearings at their top and bottom faces, and lack of bending rigidity of the fiber reinforcement sheets. At extreme lateral displacement when the originally vertical faces (end faces) of a rectangular SU-FREI bearing come in contact with top and bottom horizontal contact supports, the bearing exhibits increased lateral stiffness resulting in a stable condition. Modifications to the geometry of the end faces are expected to significantly alter the lateral response behaviour of a SU-FREI bearing. A preliminary study conducted to investigate the influence of bearing end geometry on the response behavior of a base isolated masonry building is reported in this paper. The preliminary results suggest that the bearing end geometry can be considered as a new design variable for SU-FREI bearings.

KEYWORDS: masonry building, base isolation, seismic mitigation, fiber reinforced elastomeric isolator, stable unbonded bearing, end geometry, frequency, stiffness.

INTRODUCTION

Practical problems and costs associated with improving the ductility of masonry building, using various steel reinforcement schemes, make base isolation a viable earthquake mitigation strategy for this type of buildings. However, these buildings cannot be isolated cost effectively using conventional steel reinforced elastomeric isolator (SREI) bearings [1].

Stable unbounded-fiber reinforced elastomeric isolator (SU-FREI) bearings, which are simply installed between the superstructure and foundation with no bonding at the contact surfaces provide a promising alternative for effective earthquake mitigation of masonry buildings [2, 3]. Compared to traditional SREIs, FREIs are lighter in weight with potential for significantly lower manufacturing costs. Square or rectangular FREI bearings can be cost effectively produced by cutting a large fabricated FREI sheet to the required sizes. Elimination of the thick end steel plates, which are commonly bonded to the top and bottom faces of conventional SREIs, results

in additional cost savings in FREIs. Superior damping as a result of interaction between rubber and fiber reinforcement layers justifies the use of low damped soft rubber compounds in a SU-FREI bearing subjected to relatively low vertical pressures [4]. The SU-FREI bearings, made from a soft rubber compound, can be placed underneath a shear wall type masonry superstructure with relatively close spacing (see Figure 1). Therefore, the tie-beam located at the top of the bearings to carry the superstructure does not require heavy reinforcement, and no special foundation system is required. As a result, no significant additional cost is expected to be imposed on construction of a typical masonry building isolated with SU-FREI bearings.

A SU-FREI bearing exhibits a unique stable rollover (SR) deformation characteristic due to its unbonded boundary conditions at the contact surfaces and lack of flexural rigidity of the fiber reinforcement layers. Previous studies [4, 5] have demonstrated that SR characteristic improves the seismic mitigation efficiency of a SU-FREI bearing. Results obtained from a recent study [6] suggest that a new parameter, namely, geometry of the bearing end faces, which may come in contact with the top or bottom bearing supports at the extreme bearing lateral displacements, can affect the response behaviour of a SU-FREI bearing. This new parameter is referred to hereafter as bearing end geometry. This paper reports on an investigation of SU-FREI bearings having different end geometries.

BASE ISOLATED MASONRY BUILDING

A 2-storey masonry building, shown in Figure 1, is considered as a representative prototype superstructure to be seismically isolated with SU-FREI bearings. The building is assumed to be constructed with fully grouted 20 cm, 15 MPa hollow concrete blocks. To achieve a well defined masonry structural system, each shear wall is considered to have a rectangular cross section with no openings. Intentionally, no intersections have been incorporated between the perpendicular walls. Although this structural system is somewhat simpler than a real building, its dynamic characteristics are in the same range as real masonry shear wall structures. The base isolation system, as indicated in Figure 1, employs eight identical SU-FREI bearings located underneath the superstructure.

Figure 1c contains a simple 3DOF mass-spring-dashpot model of the prototype base isolated building. The fundamental period of the non-isolated model of the masonry superstructure, shown in Figures 1a and 1b, is calculated to be 0.17 s in both the x and y directions. In this analysis, the in-plane lateral stiffness of the individual masonry shear walls due to bending and shear deformations is calculated in a model where both ends of the wall are assumed to be fixed against rotation and the wall is subjected to a horizontal in-plane load at the top of the storey. To account for cracking in the wall, an equivalent thickness [7] is evaluated based on the effective moment of inertia of $I_e = 0.35 I_g$ as suggested for cracked section properties of beams and walls in the ACI code [8]. Although the equivalent thickness of the walls (i.e., $t_e = 0.35t$) is taken into account for modelling purposes, the weight of the walls is calculated based on its full thickness. The total weight of the building, including the base diaphragm, is approximately 511 kN. Thus, each bearing is subjected to P = 64 kN vertical load.

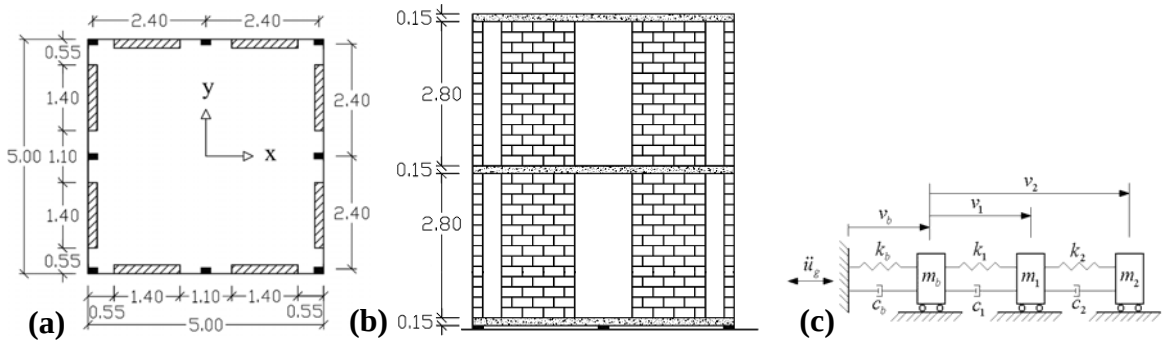

Figure 1: Prototype 2-Storey Masonry Superstructure Sitting on Eight Identical SU-FREI Bearings (All Dimensions in Meter): a) Plan View; b) Elevation View; c) Mass-Spring-Dashpot Idealization of the Base Isolated System

BEARING ISOLATORS

The performance of three different SU-FREI bearings in the proposed base isolation system is studied in this paper. The bearings are designated FRB1 to FRB3. All of the bearings have the same b = 124 mm width but their end geometries are different (see Table 1). The aspect ratio, R, (defined as the ratio of length to height of the bearing) and shape factor, S, (defined as the ratio of plan area to circumferential area for one rubber layer in the bearing) of the bearings are listed in Table 1. The shape factor highly affects the effective compression modulus of a bearing under a specified level of vertical load and the aspect ratio affects the nature of the Stable Rollover deformation in SU-FREI bearings [5].

Table 1: Sketch and Geometry of the SU-FREI Bearings

Bearing	Side View	h (mm)	L (mm)		R=L/h	S
			L_{inner}	L_{outer}		
FRB1	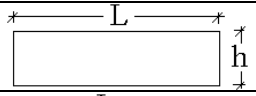	96	304		3.2	6.9
FRB2	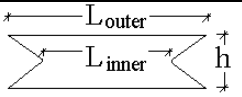	92	208	296	2.2-3.2	6.1-6.9
FRB3	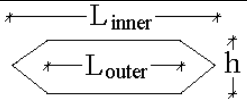	92	296	208	2.2-3.2	6.1-6.9

The lateral load-displacement characteristics and damping ratios of the bearings listed in Table 1 were extrapolated from cyclic shear tests that were conducted under a constant vertical load on ¼ scale models of these bearings [6]. The level of vertical load applied on the model scale bearings simulated the corresponding full scale value of P = 64 kN. All of the tested model scale bearings were fabricated from alternating layers of soft neoprene and bi-directional carbon fiber fabric. A detailed description and results of the experimental program can be found in Reference [6].

The variations of secant lateral stiffness and equivalent damping ratio with respect to the bearing lateral displacement are shown in Figures 2a and 2b, respectively, for full scale Bearings FRB1 to FRB3. As shown in these figures, compared to other tested bearings Bearing FRB1 had the largest stiffness values over the entire range of lateral displacements. At lateral displacements lower than 75 mm the stiffness of Bearing FRB2 was found to be slightly lower than that of Bearing FBR1. However, at larger displacements these two bearings showed similar stiffness values. In addition, both Bearings FRB1 and FRB2 showed comparable damping ratios over the investigated range of lateral displacements with the exception of the lowest displacement value where Bearing FRB2 exhibited a higher energy dissipation capability. Test results indicated that at lateral displacements lower than 75 mm Bearing FRB3 was significantly more flexible than other tested bearings. However, at larger displacements when the bearing lateral faces came in contact with the top and bottom supports, the bearing stiffness approached those of Bearings FRB1 and FRB2. Compared to all other tested bearings, FRB3 generally maintained larger damping values with the exception of the lowest displacement value [6].

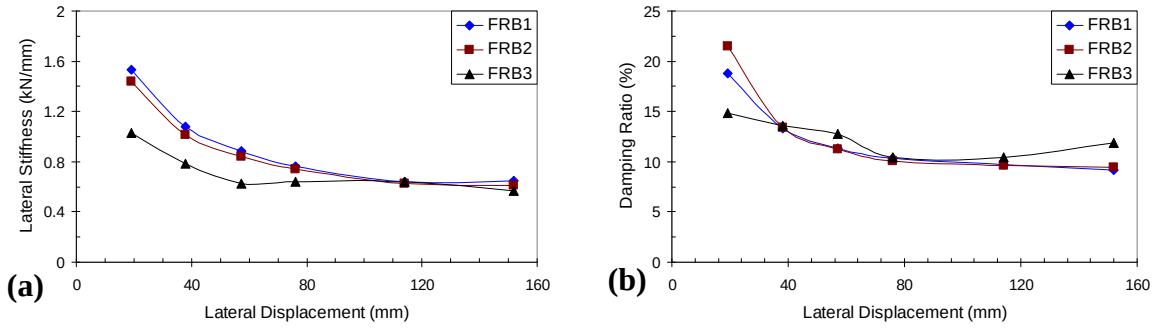

Figure 2: Response Properties of the Isolators: a) Lateral Stiffness; b) Damping Ratio

MODELING OF THE BASE ISOLATED SYSTEM

The governing equations of motion for the mass-spring dashpot model, shown in Figure 1c, are as follows [1]:

$$\mathbf{M}^*\ddot{\mathbf{V}}^* + \mathbf{C}^*\dot{\mathbf{V}}^* + \mathbf{K}^*\mathbf{V}^* = -\mathbf{M}^*\mathbf{r}^*\ddot{u}_g \tag{1}$$

Where,

$$\mathbf{M}^* = \begin{bmatrix} m+m_b & \mathbf{r}^T\mathbf{M} \\ \mathbf{M}\mathbf{r} & \mathbf{M} \end{bmatrix}, \qquad \mathbf{C}^* = \begin{bmatrix} c_b & \mathbf{0} \\ \mathbf{0} & \mathbf{C} \end{bmatrix}, \qquad \mathbf{K}^* = \begin{bmatrix} k_b & \mathbf{0} \\ \mathbf{0} & \mathbf{K} \end{bmatrix} \tag{2}$$

$$\mathbf{r} = \begin{Bmatrix} 1 \\ 1 \end{Bmatrix}, \qquad \mathbf{r}^* = \begin{Bmatrix} 1 \\ \mathbf{0} \end{Bmatrix}, \qquad \mathbf{V}^* = \begin{Bmatrix} v_b \\ \mathbf{v} \end{Bmatrix}, \qquad m = m_1 + m_2 \tag{3}$$

where, **M**, **C**, and **K** are mass, damping, and stiffness matrices of the non-isolated model of the superstructure, respectively. The vertical component of ground motion has been ignored in this analysis. Additionally, given the fact that the applied vertical pressure on each bearing is

significantly below the buckling pressure, the small influence of variation in vertical pressure on the lateral response characteristics of the bearings has been neglected.

In the proposed analysis, since the masonry superstructure remains nearly rigid and uncracked it has been treated as a linear elastic system with 2% equivalent viscous damping. However, in order to account for a conservatively largest response in the superstructure, the stiffness of this linear model has been evaluated based on cracked section properties of the masonry shear walls (i.e., $I_e = 0.35 I_g$ and $t_e = 0.35 t$). To study the dynamic response of the corresponding non-isolated building, the same linear stiffness properties of the superstructure in conjunction with a typical 5% damping ratio have been taken into account in the analysis.

The lateral load, $f_{b,i}$ that is resisted by an individual SU-FREI bearing "*i*" in the base isolation system can be attributed to the sum of the stiffness and damping forces as follows:

$$f_{b,i}(t) = f_{sb,i}(t) + f_{db,i}(t) \tag{4}$$

where, the stiffness force, $f_{sb,i}(t)$, of each bearing can be calculated from the secant lateral stiffness, $k_{b,i}(v_b(t))$, and lateral displacement, $v_b(t)$, of the bearing as follows:

$$f_{sb,i}(t) = k_{b,i}(v_b(t))\, v_b(t) \tag{5}$$

In a simple approach, the secant lateral stiffness, $k_{b,i}$, of each bearing, is modeled as a fourth order polynomial given by

$$k_{b,i}(v_b(t)) = b_0 + b_1 v_b(t) + b_2 v_b^2(t) + b_3 v_b^3(t) + b_4 v_b^4(t) \tag{6}$$

The 5 parameters b_0 to b_4 in Equation 6 are constants determined by applying a least squares fit to the experimentally evaluated lateral load-displacement hysteresis loops of the prototype SU-FREI bearings.

Results obtained from experimental tests on the model scale bearings indicated that during the first of three cycles applied with constant displacement amplitude, unscragged bearings exhibited larger lateral load resistances and damping ratios than in the two subsequent cycles [6]. Since the maximum possible value of the lateral load that is generated in the bearings is of most concern in the proposed analysis, the stiffness force, $f_{sb,i}(t)$, of each bearing has been conservatively modelled based on the unscragged bearing response at the peak lateral displacement calculated in the time history analysis. This is accomplished by fitting the polynomial of Equation 5 (also called the backbone-curve) to only the first cycles of the hysteresis loops at each level of lateral displacement.

As a typical example, Figure 3a shows the unscragged (1st cycle) lateral load-displacement hysteresis loops of one of the SU-FREI bearings at six different displacement amplitudes ranging from 0.25 t_r to 2 t_r (where, t_r = 76 mm indicates the total thickness of the rubber layers in each bearing). Curve 6 in this figure is a backbone-curve fitted to all of the unscragged loops to

provide an estimate for $f_{sb,i}(t)$ developed in the bearing. Due to increasing tangent stiffness at the maximum tested displacement, 2 t_r, the peak lateral load is accurately predicted by Curve 6 at this extreme lateral displacement amplitude. However, if the peak lateral displacement amplitude of the bearing, calculated by time history analysis is significantly less than $2t_r$, the maximum lateral load will be underestimated by Curve 6 (see Figure 3a). Therefore, the model should be modified in order to simulate the increased tangent stiffness of the hysteresis loops at peak displacement amplitudes less than 2 t_r. Figure 3b shows a set of backbone-curves (Curves 1 to 6) each fitted to the first cycle hysteresis loops shown in Figure 3a, up to a specified level of lateral displacement. For example, Curve 5 has been fitted to the all of first cycle hysteresis loops from 0.25 t_r up to 1.5 t_r lateral displacement. The *b*-parameters relevant to Curves 1 to 6 for all of the bearings listed in Table 1 are presented in Table 2.

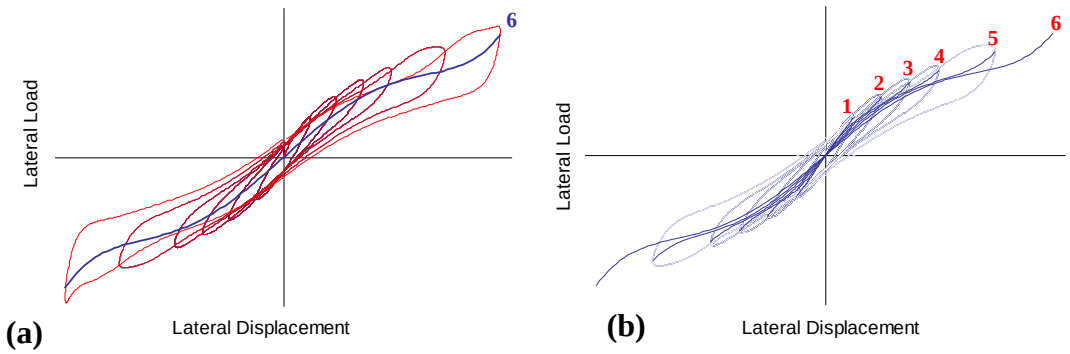

Figure 3: Typical Lateral Response of SU-FREI Bearings: a) Unscragged Lateral Load-Displ. hysteresis loops; b) Backbone Curves Simulating the Stiffness force of the Bearings

In a dynamic analysis, the mathematical hysteresis loops of the bearing can be constructed using a Rayleigh damping model as follows:

$$f_{db,i}(t) = c_{b,i}(t)\dot{v}_b(t) \tag{7}$$

where, at any time instant the damping coefficient of each bearing, $c_{b,i}(t)$, is calculated based on a constant equivalent viscous damping ratio of ξ, tributary mass m_i of the structure on each bearing, , and secant lateral stiffness of the bearing $k_{bi}(v_b(t))$ so that

$$c_{b,i}(t) = 2\xi\sqrt{k_{b,i}(v_b(t))\,m_i} \tag{8}$$

As a conservative approach ξ was selected to represent the minimum calculated damping ratio of the bearing corresponding to the three test cycles that were applied at each displacement level. Since the base-isolated system employs eight identical bearings, its lateral stiffness k_b and damping coefficient c_b, to be used in Equation 2, are eight times larger than $k_{b,i}$ and $c_{b,i}$, respectively.

Table 2: b-Parameter Values of the SU-FREI Bearings

Bearing	Backbone Curve	ξ (%)	b_0	b_1	b_2	b_3	b_4
FRB1	1	19	3.72336E-01	4.42609E-03	-1.34417E-04	-8.79325E-06	1.86740E-07
	2	13	3.47809E-01	1.64951E-03	-1.83473E-04	-9.31497E-07	8.42272E-08
	3	11	2.89273E-01	6.85842E-04	-6.37983E-05	-1.71213E-07	1.21582E-08
	4	10	2.52909E-01	4.06205E-04	-3.16341E-05	-6.07270E-08	3.27924E-09
	5	10	2.24732E-01	1.70932E-04	-1.67426E-05	-1.04137E-08	8.38943E-10
	6	9	1.98747E-01	1.02353E-04	-1.00700E-05	-3.95258E-09	3.35495E-10
FRB2	1	20	3.41730E-01	-3.43244E-04	-9.20322E-05	1.53605E-06	1.07569E-07
	2	13	3.21177E-01	9.77805E-05	-1.69971E-04	2.21389E-08	8.10843E-08
	3	11	2.66392E-01	7.83927E-06	-5.67209E-05	1.28174E-10	1.12196E-08
	4	10	2.33491E-01	-1.98286E-06	-2.80806E-05	-1.83975E-09	3.06615E-09
	5	10	2.07194E-01	-2.96100E-05	-1.41209E-05	2.31946E-09	7.14250E-10
	6	9	1.83774E-01	-4.12724E-05	-8.38813E-06	2.72724E-09	2.76645E-10
FRB3	1	15	2.72856E-01	-7.95133E-03	-1.52871E-04	1.72631E-05	1.47363E-07
	2	14	2.38308E-01	-2.01940E-03	-1.13866E-04	1.25276E-06	5.51820E-08
	3	13	2.00402E-01	-8.34647E-04	-3.98340E-05	2.20582E-07	7.17544E-09
	4	10	1.85847E-01	-3.78397E-04	-3.32215E-05	3.39975E-08	4.66684E-09
	5	10	1.42348E-01	-3.24014E-04	-5.20709E-06	2.29812E-08	4.33330E-10
	6	12	1.23421E-01	-1.78038E-04	-4.39209E-07	7.33262E-09	2.06361E-11

Note: The maximum bearing lateral displacement for Curves 1 to 6 are 0.25, 0.5, 0.75, 1, 1.50, and 2 t_r, respectively.

In the time history analysis presented in this paper, the appropriate values of the *b*-parameters together with a proper viscous damping ratio are determined through an iterative approach. The following is a description of the iterative approach employed.

i) The *b*–parameters together with the damping ratio of Curve 6 are initially used to model the bearings' lateral load-displacement hysteresis loops.
ii) Time history analysis of the base-isolated structure is carried out and the peak amplitude of the bearings' lateral displacement ($v_{b,\max}$) is calculated.
iii) The new *b*-parameters and ξ-value are calculated from Table 2 through linear interpolation between the values corresponding to the lateral displacement levels that bracket the current $v_{b,\max}$.
iv) The value of $v_{b,\max}$ is updated through repeating the time history analysis on the base-isolated structure.
v) This iterative process is continued until $v_{b,\max}$ converged to its unique value with sufficient accuracy.

Using this technique, in the time history analysis described in the next section, the convergence of $v_{b,\max}$ with an accuracy of ±1% t_r, was achieved after 3 to 4 iterations.

SELECTED SEISMICITY AND INPUT EARTHQUAKE

Time history analysis was employed to demonstrate the seismic mitigation effectiveness of the proposed SU-FREI bearings with different end geometries. The acceleration time history for the NS component of El Centro 1940 earthquake was selected and scaled by a factor of 1.32 to match its Peak Ground Acceleration (PGA) to the maximum expected value (with 2%

probability of exceedence within 50 years) for Vancouver, namely 0.46g (NBCC, 2005). Comparison between the 5% damped pseudo acceleration spectrum of this earthquake and the design spectrum for Vancouver (for site class C (very dense soil or soft rock) as defined by NBCC, 2005) showed that for the periods longer than approximately 0.2 s, the input earthquake exceeded the expected level of seismic hazard.

TIME HISTORY ANALYSIS: PEAK RESPONSE VALUES AND DISCUSSION

Using the selected input earthquake and the iterative time history analysis approach discussed in this paper, response histories of the masonry building isolated using the three different bearings were evaluated. In addition, a time history analysis on the corresponding non-isolated building was carried out to highlight the seismic mitigation efficiency of the proposed base isolation system. Table 3 lists the peak response values as the outcomes of the time history analyses. As can be seen in Table 3 in general, regardless the type of the SU-FREI used in the base isolation system, significant attenuation occurred in response parameters such as floor acceleration, inter-storey drift, base shear, and overturning moment of the masonry superstructure compared to those of the corresponding non-isolated building.

Table 3: Peak Response Values in Non-Isolated and Different Base-Isolated Systems

Masonry Building	Bearings	Max. Bearings' Lateral Displ. *(mm)*	Absolute Accel. *(g)*		Inter-Storey Drift *(mm)*		Base Shear *(kN)*	Overt. Moment *(kN.m)*
			1st Floor	Roof	1st Floor	Roof		
Non-Isolated	N/A	N/A	0.78	1.16	5.70	3.00	334	1462
Base-Isolated	FRB1	108	0.30	0.30	1.84	0.78	108	462
	FRB2	107	0.29	0.30	1.80	0.76	106	453
	FRB3	103	0.29	0.30	1.80	0.76	106	453

As shown in Table 3 the seismic mitigation achieved, using Bearings FRB1 or FRB2 in the base isolation system, is similar. The maximum lateral displacement experienced by these bearings is within the displacement range where both bearings have similar stiffness and damping values (see Figure 2). An inspection of Figure 2a indicates that for moderate earthquakes that impose lateral displacements lower than 75 mm on the bearings, Bearing FRB2 has lower stiffness values and higher or equivalent damping ratios compared to Bearing FRB1. Therefore, it is anticipated that the performance of Bearing FRB2 will be more effective than Bearing FRB1 for moderate earthquakes.

Despite different lateral response characteristics of Bearing FRB3, for the given input earthquake the peak response values of a base isolation system constructed from Bearings FRB3 were found to be comparable with those of Bearings FRB1 and FRB2 (see Table 3). As shown in Table 3, the maximum lateral displacement in Bearing Type FRB3 was calculated to be 103 mm. An inspection of Figure 2 indicates that for this level of lateral displacement, the response characteristics (stiffness and damping) of Bearing FRB3 is similar to FRB1. As a result, for the given input earthquake and the resulting level of lateral displacement, the seismic isolation performance of these three bearings was comparable. Due to its significantly reduced lateral stiffness, the seismic isolation efficiency of Bearing FRB3 is expected to be considerably higher than Bearings FRB1 and FRB2 for lateral displacements lower than 75 mm (see Figure 2a).

Also, the relatively higher damping ratios of Bearing FRB3 at lateral displacements larger than 120 mm implies that this bearing will exhibit lower displacements compared to Bearings FRB1 and FRB2, when it is subjected to more intensive excitations.

CONCLUSIONS

Stable unbonded-fiber reinforced elastomeric isolator (SU-FREI) bearings are considered as potentially cost-effective isolators for seismic mitigation of typical low-rise masonry structures. In the case of a shear wall masonry building, these bearings can be simply placed underneath the superstructure with relatively close spacing. The close spacing of the bearings eliminates the need for special structural elements or foundation system. If any, only minor additional cost would be required for the construction of this base isolation system.

The concept of modifying the end geometry of SU-FREI bearings was investigated in this paper. A base isolation system comprising eight SU-FREI bearings was used for seismic mitigation of an ordinary masonry building. Three bearings with different end geometries were investigated. The bearings investigated included one rectangular bearing with vertical end faces and two bearings with modified end geometries. All bearings had the same material properties, number of rubber and reinforcement layers, width, and height. The lateral response characteristics of the full scale bearings were extrapolated from the experimentally-evaluated response values of their corresponding ¼ scale model.

A comparison of the bearings' lateral stiffness values and damping ratios corresponding to different bearing displacement levels indicated that modifications in end geometry could significantly alter the bearing lateral response. Seismic mitigation efficiency of the bearings with modified end geometry would highly depend on the level of displacement imposed on the bearing by the input excitation. For the input earthquake considered in this study, results of iterative nonlinear time history analyses indicated that the peak response values of the bearings with modified end geometry could be similar to that of the rectangular bearing.

The findings of this preliminary study indicate that the end geometry of a SU-FREI bearing can be considered as a new design parameter. Further analytical and experimental studies are required to determine the optimal end geometries that result in desirable seismic mitigation efficiency of SU-FREI bearings.

ACKNOWLEDGEMENTS

This research was carried out as part of the mandate of the McMaster University Centre for Effective Design of Structures funded through Ontario Research and Development Challenge Fund. The authors also would like to gratefully acknowledge the Ministry of Science, Research and Technology (MSRT) of Iran and the Natural Sciences and Engineering Research Council of Canada (NSERC).

REFERENCES

1. Naiem, F., and Kelly, J. M. (1999) "Design of seismic isolated structures" John Wiely & Sons, Inc., New York.
2. Toopchi-Nezhad H., Tait M. J., and Drysdale R. G. (2007) "Base isolation of small low-rise buildings using fiber reinforced elastomeric bearings" CSCE Annual General Meeting & Conference, Yellowknife, Northwest Territories, Canada, on CD-ROM.
3. Toopchi-Nezhad H., Tait M. J., and Drysdale R. G. (2008) "A novel base isolation system for seismic mitigation of low-rise buildings" The 14th World Conference on Earthquake Engineering, Beijing, China, on CD-ROM.
4. Toopchi-Nezhad H., Tait M. J., and Drysdale R. G. (2008) "Lateral Response Evaluation of Fiber Reinforced Neoprene Seismic Isolators" *Journal of Structural Engineering*, *ASCE*, Vol. 134, No. 10, Pages 1627-1638.
5. Toopchi-Nezhad H., Tait M. J., and Drysdale R. G. (2008) "Testing and Modeling of Square Carbon Fiber Reinforced Elastomeric Seismic Isolators" *Struct. Control and Health Monit.*, Vol. 15, No. 6, Pages 876-900.
6. Tait M. J., Toopchi-Nezhad H., and Drysdale R. G. (2008) "Influence of End Geometry on Fiber Reinforced Elastomeric Isolators" The 14th World Conference on Earthquake Engineering, Beijing, China, on CD-ROM.
7. Tokoro, K. A. T., Anderson J. C., and Bertero, V. V. (2004) "Seismic Performance of Masonry Buildings and Design Implications" PEER Report 2004/01, Pacific Earthquake Engineering Research Center College of Engineering, University of California, Berkeley.
8. American Concrete Institute (2002) "Building Code Requirements for Structural Concrete and Commentary" ACI 318-02.